



OPEN

Multifunctional Interface Modification of Energy Relay Dye in Quasi-solid Dye-sensitized Solar Cells

SUBJECT AREAS:

SOLAR CELLS

ELECTRONIC MATERIALS

Rui Gao¹, Yixiu Cui¹, Xiaojiang Liu¹ & Liduo Wang²

Received

31 March 2014

Accepted

13 June 2014

Published

4 July 2014

Correspondence and requests for materials should be addressed to R.G. (gaorui_2013@tsinghua.org.cn) or L.D.W. (chldwang@mail.tsinghua.edu.cn)

¹Institute of Electronic Engineering, China Academy of Engineering Physics, Mianyang 621900, Sichuan, China, ²Key Lab of Organic Optoelectronics & Molecular Engineering of Ministry of Education, Department of Chemistry, Tsinghua University, Beijing 100084, China.

In this paper, 4-(dicyanomethylene)-2-t-butyl-6(1,1,7,7-tetramethyljulolidyl-9-enyl)-4H-pyran (DCJTb) has been used in interface modification of dye-sensitized solar cells (DSCs) with combined effects of retarding charge recombination and Förster resonant energy transfer (FRET). DCJTb interface modification significantly improved photovoltaic performance of DSCs. I–V curves shows the conversion efficiency increases from 4.27% to 5.64% with DCJTb coating. The application of DCJTb with combined effects is beneficial to explore more novel multi-functional interface modification materials to improve the performance of DSCs.

Since 1991, dye-sensitized solar cells (DSCs) have attracted much attention worldwide due to its lower production cost and easier fabrication¹. Much work has been done on dye molecules^{2,3}, photoanode⁴, electrolyte⁵ and counter electrode⁶ to improve the photovoltaic performance of DSCs. Now the highest conversion efficiency over 12% has been achieved⁷.

In DSCs, the interface between sensitized TiO₂ and electrolyte plays a vital role in the photovoltaic performance^{8,9} as several important reactions or processes occur here, such as electron injection, charge transfer, charge recombination and dye regeneration. Interface modification and additives in electrolyte have been demonstrated effective ways to enhance the conversion efficiency and improve the stability of DSCs^{10–15}. Earlier studies focused mainly on control and modification of metal oxide¹⁴ or carboxylate¹³. Such work improved the performance of DSCs mainly through retarding the charge recombination. Recently, a new kind of interface modification material has been developed to improve the performance of DSCs, which acts as energy relay dye (ERD) that could enhance the photoresponse through Förster resonant energy transfer (FRET) effect, in addition to retarding surface charge recombination¹⁶.

FRET involves dipole–dipole coupling of ERD and acceptor through an electric field, which has been applied in DSCs and polymer solar cells to enhance their photoresponse and obtained excellent results¹⁷. FRET also occurs between quantum dots and organic dyes, which improves the photo capture^{18–20}. Excitation of ERD could be non-radiative transfer to the acceptor dye through the electric field as the emission spectrum of the ERDs overlaps with the absorption spectrum of acceptors^{21–23}. FRET efficiency between ERDs and acceptors mostly depended on the Förster radius (R_0). ERDs applied in DSCs were commonly dispersed in the liquid electrolyte²⁴. In such a configuration, many ERD molecules cannot transfer energy effectively as they were far away from the acceptor dyes attached on the TiO₂ surface. Furthermore, the solvent could cause the ERDs elicitation quenching. Assembling ERDs on the interface would avoid such disadvantages as they are concentrated at the interface of sensitized photoanode and electrolyte^{25–26}. The distance between ERDs and acceptors is short and the contact of ERD and solvent in electrolyte is minimized or avoided as well.

In this paper, 4-(dicyanomethylene)-2-t-butyl-6(1,1,7,7-tetramethyljulolidyl-9-enyl)-4H-pyran (DCJTb) has been applied as ERD in DSCs, which was widely used in organic light emitting diode (OLED)²⁷, but has never been explored in DSCs. N3 dye was used as the acceptors. Absorption peak of N3 well overlapped with the emission peak of DCJTb, assuring the effective FRET between them. Using DCJTb in the interface modification, photovoltaic performance of DSCs has been improved due to DCJTb's combining effects of FRET and retarding charge recombination.



Experimental

The TiO₂ colloid was prepared with a hydrothermal method, which has been well documented in the previous report²⁸. To prepare porous TiO₂ film, transparent conductive FTO glass (12Ω square⁻¹) was thoroughly cleaned and a thin compact TiO₂ film (about 8 nm in thickness) was subsequently deposited on the FTO by dip coating in order to improve ohmic contact and adhesion between the following porous TiO₂ layer and the conductive FTO glass. The doctor blade technique was then adopted to prepare the porous TiO₂ layer, the thickness of the porous layer being controlled by an adhesive tape. Afterwards, the film was thermo-treated at 450 °C for 30 min. When cooled to 110 °C, the TiO₂ electrode was sensitized by immersion in 0.3 mmol L⁻¹ N3 absolute ethanol solution for 12 h and cleaning with absolute ethanol. Coating of DCJT B was performed as follows: the saturated ethanol solution of DCJT B was dipping on the sensitized TiO₂ film, then dried in air for 30 min to make it concentrated on the surface of TiO₂ film. The N3 sensitizer was commercially available. DCJT B has been synthesized as in the Ref. 29.

The preparation procedure for the polymer gel electrolytes includes two steps. First, liquid electrolyte was prepared. Second, poly (ethylene oxide) (PEO) was slowly added into the liquid electrolyte and heated under strong stirring until the polymer gel electrolyte became homogeneous. The composition of the liquid electrolyte is as follows: 0.1 mol L⁻¹ LiI, 0.1 mol L⁻¹ I₂, 0.6 mol L⁻¹ 1,2-dimethyl-3-propyl imidazolium iodide (DMP II), and 0.45 mol L⁻¹ N-methyl-benzimidazole (NMBI). The solvent was 3-methoxypropionitrile (MePN)³⁰; the weight ratios (versus liquid electrolyte) for the PEO in the electrolyte was 10.0%.

A chemically platinized conductive glass was used as the counter electrode. When assembling the DSCs, the polymer gel electrolyte was sandwiched by a sensitized TiO₂ electrode and a counter electrode with two clips; the space between the two electrodes was controlled by an adhesive tape with a thickness of 30 μm. Finally, the DSCs were baked at 80 °C to ensure the polymer could penetrate into the nanoporous electrode.

The UV-Vis reflectance absorption spectra were measured with a Hitachi U-3010 spectroscope. The Photocurrent-voltage (I-V), EIS, IMVS and IMPS were investigated by ZAHNER CIMPS electrochemical workstation. The incident photon-to-current conversion efficiency (IPCE) was measured by using a lab-made IPCE setup in Professor Meng's laboratory in Institute of Physics, Chinese Academy of Sciences.

Results and discussion

Figure 1 shows the UV-vis absorption spectra of N3, DCJT B and emission spectrum of DCJT B in solutions and adsorbed on TiO₂ film. One can see from Figure 1(a) that the emission peak of DCJT B differed from the adsorption peak of N3 in the solution, which are 620 nm and 530 nm, respectively. However, Figure 1 (b) reveals that the emission peak of DCJT B shifts to 560 nm when assembled on the TiO₂ surface, which is the same situation in the DSCs devices as using the dip-coating method to concentrate ERD at the interface of photoanode and electrolyte. Such a good overlap would promote effective FRET between them. The shift of emission peak could be attributed to the aggregation or close assembly of the DCJT B molecules on the surface of TiO₂ film. Besides, the emission peak of DCJT B on the TiO₂ surface also becomes much narrower, which is due to the aggregation-induced emission effect³¹.

The Förster radius (R_0) is the distance that FRET is 50% probable between ERD and acceptors. It could be calculated using equation (1)³².

$$R_0^6 = \frac{9000 * \ln(10) \kappa^2 Q_D}{128 * \pi^5 n^4 N_A} \int F_D(\lambda) \epsilon_A(\lambda) \lambda^4 d\lambda \quad (1)$$

Where n is the index of refraction of the host medium, κ^2 is the orientation factor (2/3 for random orientation, which could be used

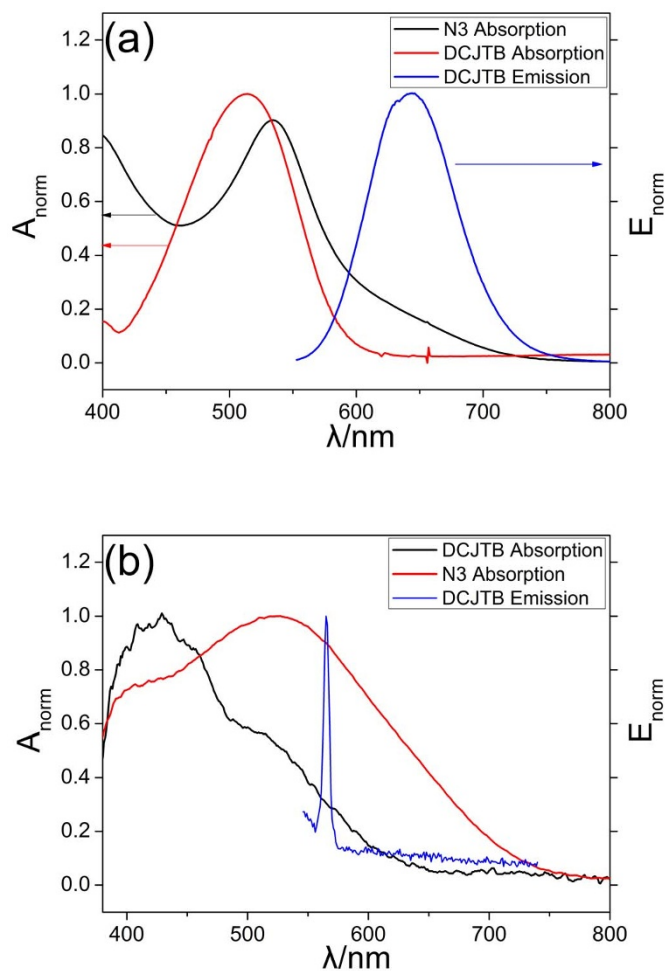


Figure 1 | UV-vis absorption spectra of N3, DCJT B and emission spectrum of DCJT B (a) in solutions and (b) on TiO₂ film.

in DSCs system), N_A is Avogadro's number, Q_D is photoluminescence efficiency of ERDs, and F_D is the emission profile of the donor. $\epsilon(\lambda)$ is the molar absorption coefficient at certain wavelength³². For the DCJT B/N3 system, it could be calculated the R_0 is 5.2 nm.

The rate of FRET between isolated chromophores has been known as point to point transfer. It is given by equation³²:

$$k_{FRET} = k_0 * \frac{R_0^6}{r^6} \quad (2)$$

where r is the separation distance between ERDs and acceptors, k_0 is the Boltzmann constant and R_0 is the Förster radius calculated from Eq 1. Equation (2) reveals that with a given R_0 , r is the most important factor that determines the efficiency of FRET³².

As shown in Figure 2 (a), adding N3 into the DCJT B solution, the emission intensity decreased to about 47.8% of the initial value. It indicates that the excitation of DCJT B has been partly transferred to N3. However, the efficiency of FRET between DCJT B and N3 is not high enough due to the much larger distance between N3 molecules and DCJT B than R_0 calculated from equation (1) in the solution system. Besides, emission peak of DCJT B and absorption peak of N3 does not overlap so well, as shown in Figure 1(a). Figure 2 (b) reveals that the emission of DCJT B almost disappeared totally when assembled on the surface of TiO₂ film, suggesting much higher energy transfer efficiency than that in the solution. It could be explained that on TiO₂ surface the distance of DCJT B and N3 has been shortened as they both are assembled on the same surface. As a result, the FRET efficiency has been enhanced significantly. Thus, the dip-coating method, which concentrates ERD and acceptors on the

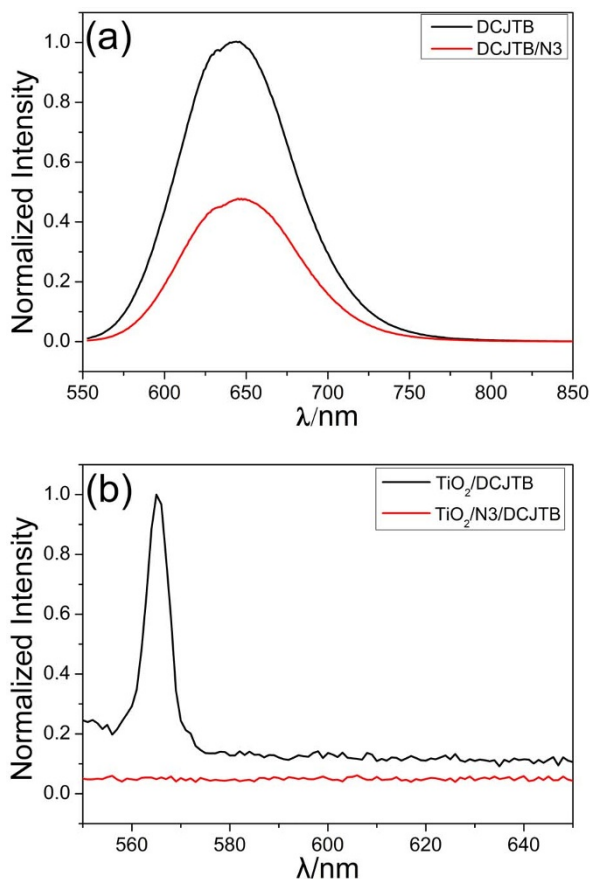


Figure 2 | (a) fluorescence emission spectra in solution (b) fluorescence emission spectra on TiO_2 film of DCJTB and DCJTB/N3.

surface of TiO_2 photoanode, has been used to obtain a better FRET efficiency in DSCs. Figure 3 shows the schematic drawing of FRET in DSCs using DCJTB as ERD and N3 as acceptors. The excitation of DCJTB transfers to N3 through FRET, and subsequently the electrons inject to the conductive band of TiO_2 , which could increase the photoresponse and photocurrent of DSCs.

As DCJTB molecules are concentrated on the surface of sensitized TiO_2 , shortening the distance between ERD and acceptors. Thus the FRET could occur more effectively than that with dispersing ERDs in the electrolyte reported in previous studies^{33–34}. Figure 4 (a) shows that with DCJTB coating on the sensitized TiO_2 film, IPCE of DSCs increased clearly in the range of 380–500 nm. This increase is attributable to the effective FRET from DCJTB to N3. And then the

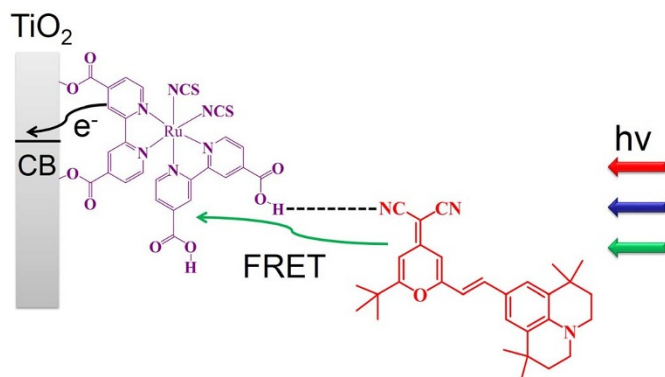


Figure 3 | Diagrammatic drawing of FRET in DSCs using DCJTB as ERD.

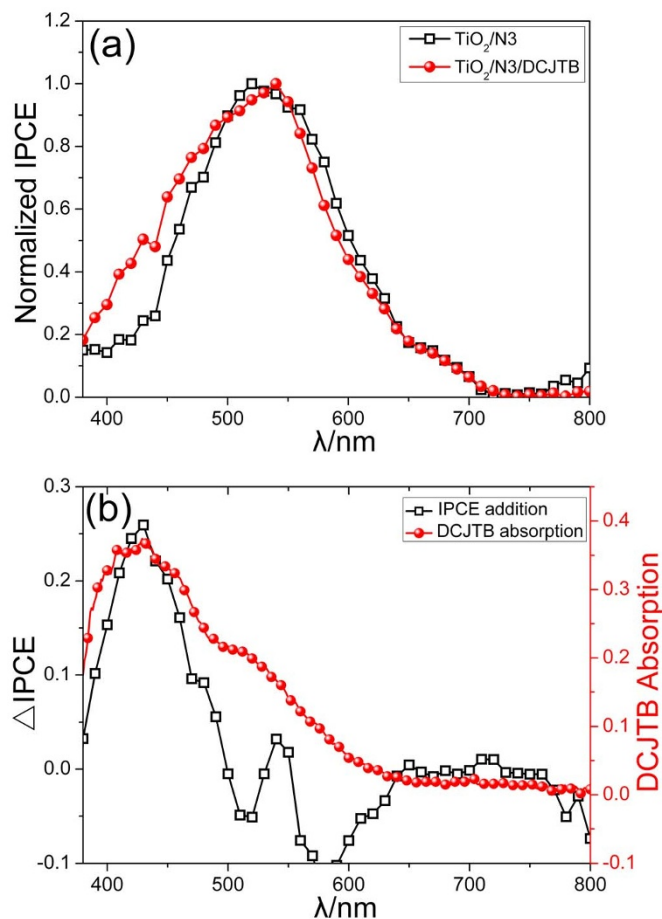


Figure 4 | (a) IPCE spectra of DSCs with and without DCJTB coating (b) comparison between additional IPCE and absorption of DCJTB.

additional electrons of N3 inject into the conductive band of TiO_2 , which could increase the photocurrent of DSCs. As revealed in Figure 4 (b), additional IPCE with DCJTB coating in the range of 380–500 nm overlaps well with the absorption peak of DCJTB. This result further indicates that FRET from DCJTB to N3 in DSCs system effectively occurred on the sensitized TiO_2 film.

The results of IPCE show that the FRET between DCJTB and N3 increased photoresponse of DSCs devices, which could enhance the photocurrent. To investigate the effects of FRET on the DSCs' photovoltaic performance, we tested the I–V curves of DSCs without and with DCJTB coating. As shown in Figure 5 (a) and Table 1, the J_{sc} increases from 12.96 without DCJTB coating to 16.63 mA/cm^2 with DCJTB coating, i.e., 28.3% enhancement in short-circuit current density. It accords with the increase of IPCE shown in Figure 4. The power conversion efficiency of DSCs with DCJTB coating was found to be increased to 5.64% from 4.27%, or relative enhancement of 32%. In the early studies reported in literature^{33–34}, the increased power conversion efficiency was mainly due to the increased J_{sc} caused by FRET between ERD and acceptors, while V_{oc} remained unchanged or even decreased. However, the present study revealed an appreciable increase in open circuit voltage, V_{oc} from 0.65 V to 0.69 V with DCJTB coating as shown Figure 5(a) and Table 1. Figure 5 (b) also showed that the dark current density appreciably decreased with DCJTB coating, indicating that the charge recombination at the electrode and electrolyte interface in DSCs was hindered by the insertion of DCJTB coating, as a barrier layer which retards the charge recombination in DSCs as its higher LUMO energy level than that of N3 as shown in Figure 6^{35–36}. To further explore the effect of retarding charge recombination in DSCs with DCJTB coating, EIS has been tested.

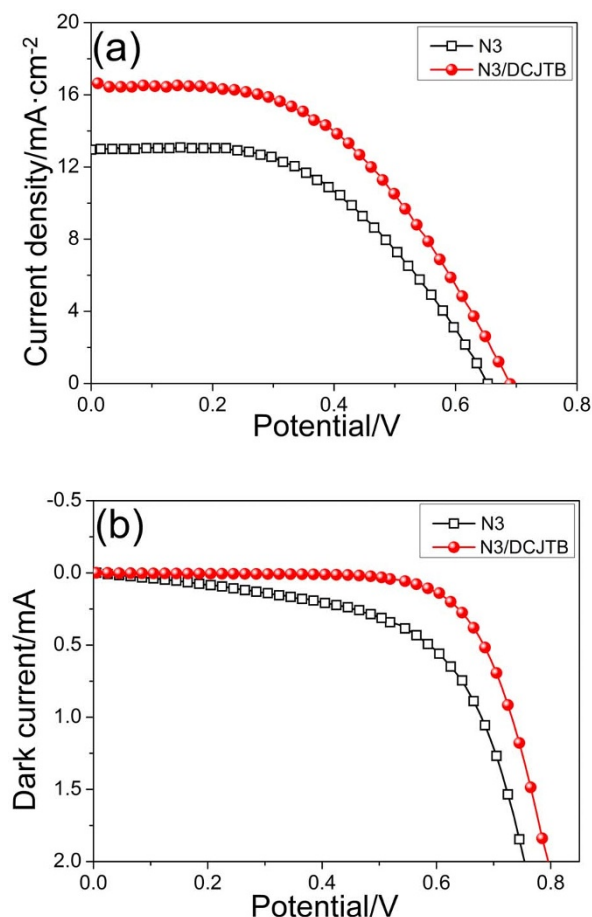


Figure 5 | (a) I–V curves under illumination of 100 mW cm^{-2} (b) Dark current curves of DSCs with and without DCJTB coating.

As shown in the equivalent circuit inserted in Figure 7 (a), the impedance associates with the charge transfer process occurring at Pt counter electrode/electrolyte interface is determined in the frequency range of 10^5 – 10^3 Hz, which is characterized by the charge transfer resistance (R_1) and the capacitance (CPE_1). In the middle frequency range of 10^3 – 10^0 Hz, the impedance representing the charge recombination process at the TiO_2 /dye/electrolyte interface is described by R_2 and the CPE_2 . In the low frequency range or 0.1–10 Hz, the Warburg diffusion impedance (Z_w) within the electrolyte is estimated. Z_w accounts for a finite length Warburg diffusion while CPE represents the constant phase element^{37–40}.

As DCJTB has been concentrated at the interface of sensitized TiO_2 and electrolyte, we focused on its effects on the charge recombination at such interface (R_2). As shown in Figure 7 (a), the charge recombination resistance increases with DCJTB coating. Thus the back reaction in DSCs has been decreased. Such result also accords with the higher V_{oc} and lower dark current shown in Figure 5. Figure 7 (b) shows the Bode pots of DSCs based on photoanode without and with DCJTB coating. The three peaks in the phase of the spectrum are associated with three transient processes in the DSC. The middle-frequency peak (in the 10–100 Hz range) is deter-

Table 1 Photovoltaic parameters of DSCs with and without DCJTB coating				
Samples	$J_{sc}/\text{mA}/\text{cm}^2$	V_{oc}/V	FF%	PCE/%
N3	12.96	0.650	50.4	4.27
N3/DCJTB	16.63	0.690	49.1	5.64

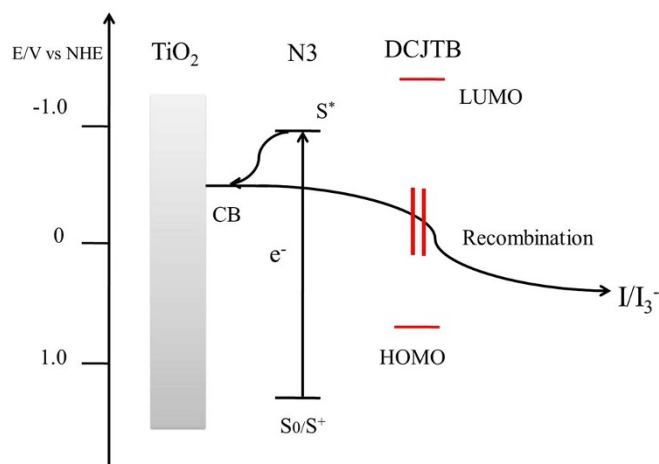


Figure 6 | Diagrammatic drawing of retarding charge recombination of DSCs with DCJTB coating.

mined by the lifetime of the electrons in TiO_2 , which is also the charge recombination time in dark condition. It is shown as follow equation⁴¹

$$\tau_r = \frac{1}{2\pi f_{\min}} \quad (3)$$

As shown in Figure 7 (b), it can be calculated that the charge recombination time of DSCs without and with DCJTB coating are 10.01 ms

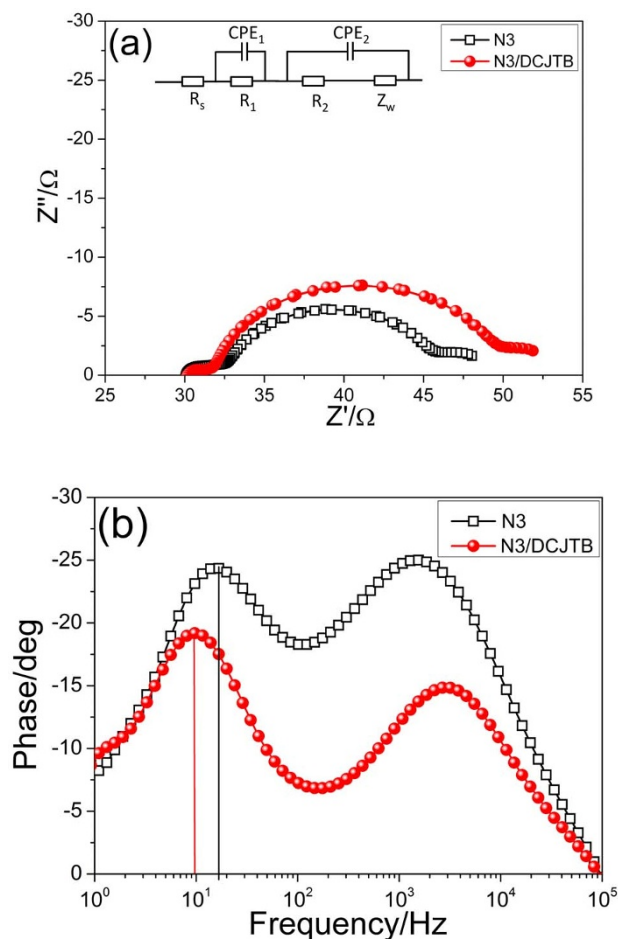


Figure 7 | (a) Nyquist plots under dark condition (b) bode plots of DSCs with and without DCJTB coating.



and 17.1 ms, respectively. As a result, it further indicates that DCJTJB could retard the interface charge recombination in DSCs devices. The V_{oc} of DSCs could be expressed by following equation^{42–43}:

$$V_{oc} = \frac{RT}{\beta F} \ln \left(\frac{AI}{n_0 k_b [I_3^-] + n_0 k_r [D^+]} \right) \quad (4)$$

where R is molar gas constant, T is temperature in Kelvin, F is Faraday constant, β is the reaction order of I_3^- and electrons, A is the electrode area surface, I is the incident photon flux, n_0 is the concentration of accessible electronic states in the conduction band. k_b and k_r are the kinetic constant of the back reaction and the recombination. $[I_3^-]$ and $[D^+]$ are concentrations of triiodide and oxidized dye, respectively. It could be considered that f_{min} is as same as the back reaction constant (k_b)⁴⁴. Thus from equation (4) it can be obtained that the longer charge recombination time causes the higher V_{oc} . It explains the increased V_{oc} shown in Figure 5 (a) and Table 1.

To further explore the influence of the DCJTJB interface modification on the electron diffusion and lifetime in DSCs under illumination, IMVS and IMPS spectra of DSCs with and without DCJTJB coating have been tested. IMVS tests the same intensity perturbation but measures periodic modulation of the photovoltage giving the information of electron lifetime under open-circuit conditions at a given illumination intensity. Figure 8 (a) shows the results of IMVS test. It indicates that the electron lifetime has been increased when the DCJTJB coating was introduced to the device, in a good agreement with retarding charge recombination as discussed earlier. IMPS measures the periodic photocurrent response to a small sinusoidal perturbation of the light intensity superimposed on a larger steady background level, which could provide information of the dynamics of charge transport and back reaction under short circuit conditions under certain illumination intensity⁴⁴.

D_{eff} which represents the effective diffusion coefficient of electrons can be determined by the followed equation⁴⁵

$$D_{eff} = D_0 \times (n_{free}/n_{total}) \quad (5)$$

where n_{free} is the density of free electrons in the conduction band of TiO_2 , and n_{total} is the total density of free and trapped electrons.

As shown in Figure 8 (b), the electron diffusion coefficient of device with DCJTJB coating clearly increases compared to that without DCJTJB coating. It indicates that DCJTJB coating is beneficial for electron transportation in DSCs. Such results also accord with the higher J_{sc} in DSCs based on DCJTJB coating, which is shown in Figure 5 (a) and Table 1. It could be due to the increased electron injection and decreased electron quenching and recombination, which increase the free electron in the photoanode. The increased electron injection is due to FRET between DCJTJB and N3.

To weigh the electron transport and recombination properties, charge collection efficiency (η_{coll}) derived from IMPS and MVS measurements was apparently considered as meaningful parameter. In sensitized solar cells, η_{coll} can be calculated by the followed equation⁴⁶

$$\eta_{coll} = 1 - \tau_c / \tau_d \quad (6)$$

where τ_c is the electron collection time given by IMPS test and τ_d is the electron lifetime given by IMVS test. Figure 8(c) shows the charge collection efficiency of DSCs without and with DCJTJB coating under different illumination intensity. It reveals that the charge collection efficiency increases with DCJTJB coating, indicating it is beneficial to charge collection in photoanode of DSCs.

Conclusions

DCJTJB as interface modification material has been used in DSCs, and it acts as a barrier layer retarding the charge recombination and resulted in increased photoresponse and electron injection efficiency

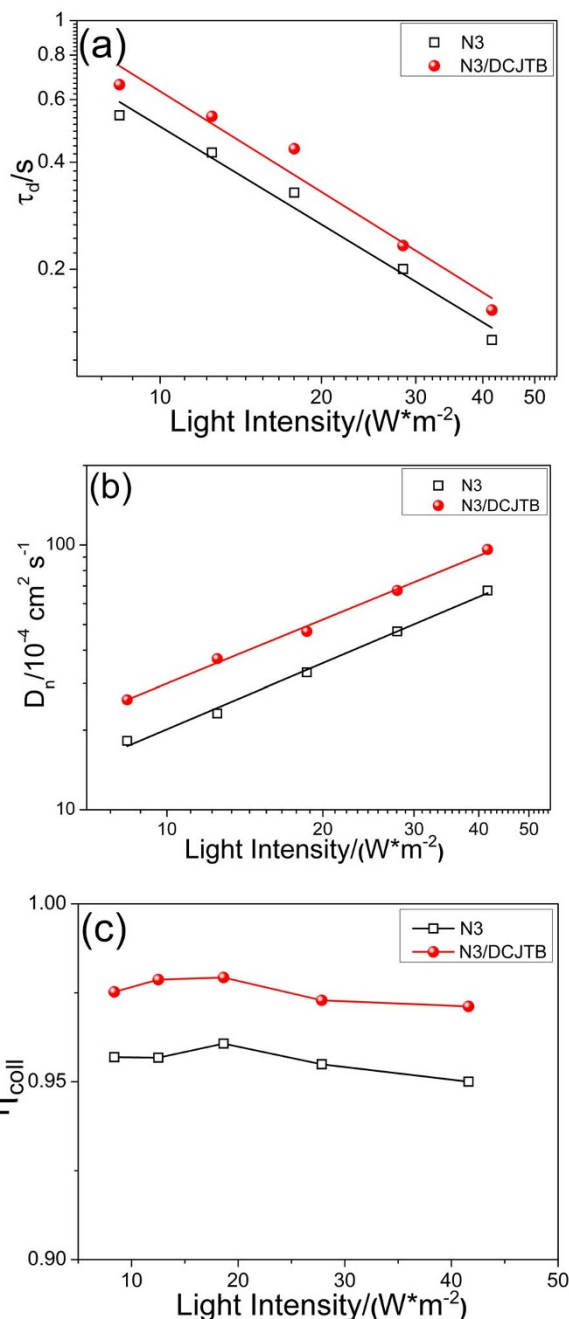


Figure 8 | (a) IMVS (b) IMPS spectra and (c) electron collection efficiency of DSCs with and without DCJTJB coating.

due to the FRET at the interface of sensitized TiO_2 and electrolyte. Dip-coating method used in interface modification avoided electron quenching by concentrate ERD and acceptors on the surface of sensitized TiO_2 . When DCJTJB assembled on the surface of TiO_2 , the distance between ERD and acceptors was reduced and thus, a higher FRET efficiency was achieved. With combining effects of retarding the charge recombination and FRET, DCJTJB interface modification has significantly improved the photovoltaic performance of DSCs.

1. O' Regan, B. & Grätzel, M. A Low-cost, high-efficiency solar cell based on dye-sensitized colloidal TiO_2 films. *Nature* **353**, 737–740 (1991).
2. Tian, H. N., Yang, X. C., Chen, R. K., Hagfeldt, A. & Sun, L. C. A metal-free “black dye” for panchromatic dye-sensitized solar cells. *Energy Environ. Sci.* **2**, 674–677 (2009).
3. Burke, A., Schmidt-Mende, L., Ito, S. & Grätzel, M. A novel blue dye for near-IR ‘dye-sensitized’ solar cell applications. *Chem. Commun.* **3**, 234–236 (2007).



4. Enache-Pommer, E., Liu, B. & Aydil, E. S. Electron transport and recombination in dye-sensitized solar cells made from single-crystal rutile TiO₂ nanowires. *Phys. Chem. Chem. Phys.* **11**, 9648–9652 (2009).
5. Lan, Z. *et al.* Template-free synthesis of closed-microporous hybrid and its application in quasi-solid-state dye-sensitized solar cells. *Energy Environ. Sci.* **2**, 524–528 (2009).
6. Lee, K. M. *et al.* Highly porous PProDOT-Et-2 film as counter electrode for plastic dye-sensitized solar cells. *Phys. Chem. Chem. Phys.* **11**, 3375–3379 (2009).
7. Yella, A. *et al.* Porphyrin-sensitized solar cells with cobalt (II/III)-based redox electrolyte exceed 12 percent efficiency. *Science* **334**, 629–634 (2011).
8. Diamant, Y., Chen, S. G., Melamed, O. & Zaban, A. Core-shell nanoporous electrode for dye sensitized solar cells: the effect of the SrTiO₃ shell on the electronic properties of the TiO₂ core. *J. Phys. Chem. B* **107**, 1977–1981 (2003).
9. Bandaranayake, K. M. P., Senevirathna, M. K. I., Weligamuwa, P. & Tennakone, K. Dye-sensitized solar cells made from nanocrystalline TiO₂ films coated with outer layers of different oxide materials. *Coord. Chem. Rev.* **248**, 1277–1281 (2004).
10. Liu, Z. Y. *et al.* Al₂O₃-coated SnO₂/TiO₂ composite electrode for the dye-sensitized solar cell. *Electrochimica Acta* **50**, 2583–2589 (2005).
11. Chen, S. G., Chappel, S., Diamant, Y. & Zaban, A. Preparation of Nb₂O₅ coated TiO₂ nanoporous electrodes and their application in dye-sensitized solar cells. *Chem. Mater.* **13**, 4629–4634 (2001).
12. Palomares, E., Clifford, J. N., Haque, S. A., Lutz, T. & Durrant, J. R. Control of charge recombination dynamics in dye sensitized solar cells by the use of conformally deposited metal oxide blocking layers. *J. Am. Chem. Soc.* **125**, 475–482 (2003).
13. Gao, R., Wang, L. D., Ma, B. B., Zhan, C. & Qiu, Y. Mg(OOCCH₃)₂ Interface Modification after Sensitization to Improve Performance in Quasi-solid Dye-Sensitized Solar Cells. *Langmuir* **26**, 2460–2465 (2010).
14. Luo, F., Wang, L. D., Ma, B. B. & Qiu, Y. Post-modification using aluminum isopropoxide after dye-sensitization for improved performance and stability of quasi-solid-state solar cells. *J. Photochem. Photobiol. A: Chem.* **197**, 375–381 (2008).
15. Fischer, A. *et al.* Crystal formation involving 1-methylbenzimidazole in iodide/triiodide electrolytes for dye-sensitized solar cells. *Sol. Energy Mater. Sol. Cells* **91**, 1062–1065 (2007).
16. Gao, R. *et al.* Interface modification of 8-hydroxyquinoline aluminium with combined effects in quasi-solid dye-sensitized solar cells. *Phys. Chem. Chem. Phys.* **14**, 5973–5978 (2012).
17. Forster, T. 10th spiers memorial lecture-transfer mechanism of electronic excitation. *Discuss. Faraday Soc.* **27**, 7–17 (1959).
18. Algar, W. *et al.* Emerging non-traditional Förster resonance energy transfer configurations with semiconductor quantum dots: Investigations and applications. *Coord. Chem. Rev.* **263–264**, 65–85 (2014).
19. Lee, E., Kim, C. & Jang, J. High-performance Förster resonance energy transfer (FRET)-based dye-sensitized solar cells: rational design of quantum dots for wide solar-spectrum utilization. *Chem.-Eur. J.* **19**, 10280–10286 (2013).
20. Sarkar, S. *et al.* Dual-Sensitization via Electron and Energy Harvesting in CdTe Quantum Dots Decorated ZnO Nanorod-Based Dye-Sensitized Solar Cells. *J. Phys. Chem. C* **116**, 14248–14256 (2012).
21. Cheon, J. H. *et al.* Enhancement of light harvesting in dye-sensitized solar cells by using Förster-type resonance energy transfer. *Met. Mater. Int.* **19**, 1365–1368 (2013).
22. Cheon, J. H. *et al.* Enhanced light-harvesting efficiency by Förster resonance energy transfer in quasi-solid state DSSC using organic blue dye. *Electrochim. Acta* **68**, 240–245 (2012).
23. Basham, J. I. *et al.* Förster Resonance Energy in Dye-Sensitized Solar Cells. *ACS Nano* **4**, 1253–1258 (2010).
24. Hardin, B. E. *et al.* High Excitation Transfer Efficiency from Energy Relay Dyes in Dye-Sensitized Solar Cells. *Nano. Lett.* **10**, 3077–3083 (2010).
25. Gao, R. *et al.* Effects of an Intercalation Nanocomposite at the Photoanode/Electrolyte Interface in Quasi-Solid Dye-Sensitized Solar Cells. *J. Phys. Chem. C* **115**, 17986–17992 (2011).
26. Gao, R. *et al.* Interface modification effects of 4-tertbutylpyridine interacting with N3 molecules in quasi-solid dye-sensitized solar cells. *Phys. Chem. Chem. Phys.* **13**, 10635–10640 (2011).
27. Shi, J. M. & Tang, C. W. Doped organic electroluminescent devices with improved stability. *Appl. Phys. Lett.* **70**, 1665–1667 (1997).
28. Shklover, V., Ovchinnikov, Y. E., Braginsky, L. S., Zakeeruddin, S. M. & Grätzel, M. Structure of Organic/Inorganic Interface in Assembled Materials Comprising Molecular Components. Crystal Structure of the Sensitizer Bis[(4,4'-carboxy-2,2'-bipyridine)(thiocyanato)] ruthenium(II). *Chem. Mater.* **10**, 2533–2541 (1998).
29. Chen, C. H., Tang, C. W., Shi, J. & Klubek, K. P. Improved red dopants for organic electroluminescent devices. *Macromolecular Symposia* **125**, 49–58 (1998).
30. Shi, Y. T. *et al.* The electrically conductive function of high-molecular weight poly(ethylene oxide) in polymer gel electrolytes used for dye-sensitized solar cells. *Phys. Chem. Chem. Phys.* **11**, 4230–4235 (2009).
31. Hong, Y., Jacky, W., Lam, Y. & Tang, B. Z. Aggregation-induced emission: phenomenon, mechanism and applications. *Chem. Commun.* 4332–4353 (2009).
32. Yum, J. H. *et al.* Incorporating multiple energy relay dyes in liquid dye-sensitized solar cells. *ChemPhysChem* **12**, 657–661 (2011).
33. Yum, J. H. *et al.* Panchromatic Response in Solid-State Dye-Sensitized Solar Cells Containing Phosphorescent Energy Relay Dyes. *Angew. Chem. Int. Ed.* **48**, 9277–9280 (2009).
34. Hardin, B. E. *et al.* Increased light harvesting in dye-sensitized solar cells with energy relay dyes. *Nat. Photonics* **3**, 406–411 (2009).
35. Tang, C. W. & Vanslyke, S. A. Organic electroluminescent diodes. *Appl. Phys. Lett.* **51**, 913–915 (1987).
36. Grätzel, M. Photoelectrochemical cells. *Nature* **414**, 338–344 (2001).
37. Wang, Q., Moser, J. E. & Grätzel, M. Electrochemical impedance spectroscopic analysis of dye-sensitized solar cells. *J. Phys. Chem. B* **109**, 14945–14953 (2005).
38. Qin, D. *et al.* Ionic liquid/polymer composite electrolytes by in situ photopolymerization and their application in dye-sensitized solar cells. *Electrochim. Acta* **56**, 8680–8687 (2011).
39. Gao, R. *et al.* Photovoltaic Properties and Mechanism Analysis of a Dye/Al₂O₃ Alternating Assembly Structure by Electrochemical Impedance Spectroscopy. *Acta. Phys.-Chim. Sin.* **27**, 413–418 (2011).
40. Gao, R., Niu, G. D., Wang, L. D., Ma, B. B. & Qiu, Y. N3/Al₂O₃/N749 Alternating Assembly Structure Broadening the Photoresponse and Interface Modification Effects in Quasi-Solid Dye-Sensitized Solar Cells. *Acta. Phys.-Chim. Sin.* **29**, 73–81 (2013).
41. Kern, R., Sastrawan, R., Ferber, J., Stangl, R. & Luther, J. Modeling and interpretation of electrical impedance spectra of dye solar cells operated under open-circuit conditions. *Electrochim. Acta* **47**, 4213–4225 (2002).
42. Lee, K., Park, S. W., Ko, M. J., Kim, K. & Park, N. G. Selective positioning of organic dyes in a mesoporous inorganic oxide film. *Nat. Mater.* **8**, 665–671 (2009).
43. Adachi, M., Sakamoto, M., Jiu, J., Ogata, Y. & Isoda, S. Determination of parameters of electron transport in dye-sensitized solar cells using electrochemical impedance spectroscopy. *J. Phys. Chem. B* **110**, 13872–13880 (2006).
44. Bisquert, J. Theory of the Impedance of Electron Diffusion and Recombination in a Thin Layer. *J. Phys. Chem. B* **106**, 325–333 (2002).
45. Dloczik, L. *et al.* Dynamic Response of Dye-Sensitized Nanocrystalline Solar Cells: Characterization by Intensity-Modulated Photocurrent Spectroscopy. *J. Phys. Chem. B* **101**, 10281–10289 (1997).
46. Hagfeldt, A., Boschloo, G., Sun, L. C., Kloo, L. & Pettersson, H. Chem. Dye-Sensitized Solar Cells. *Chem. Rev.* **110**, 6595–6663 (2010).

Acknowledgments

This work was supported by the National Natural Science Foundation of China under Grant No. 51273104 and the National Key Basic Research and Development Program of China under Grant No. 2009CB930602.

Author contributions

L.W. proposed the conceptual idea and provided financial support through grant application. G.R. participated in the analysis of results, discussing and writing the manuscript. Y.C. and X.L. participated in discussing the results and in writing the manuscript. All authors read and approved the final manuscript.

Additional information

Competing financial interests: The authors declare no competing financial interests.

How to cite this article: Gao, R., Cui, Y.X., Liu, X.J. & Wang, L.D. Multifunctional Interface Modification of Energy Relay Dye in Quasi-solid Dye-sensitized Solar Cells. *Sci. Rep.* **4**, 5570; DOI:10.1038/srep05570 (2014).



This work is licensed under a Creative Commons Attribution-NonCommercial-NoDerivs 4.0 International License. The images or other third party material in this article are included in the article's Creative Commons license, unless indicated otherwise in the credit line; if the material is not included under the Creative Commons license, users will need to obtain permission from the license holder in order to reproduce the material. To view a copy of this license, visit <http://creativecommons.org/licenses/by-nc-nd/4.0/>